



**HAL**  
open science

# Magnetic Resonance Acoustic Radiation Force Imaging (MR-ARFI) for the monitoring of High Intensity Focused Ultrasound (HIFU) ablation in anisotropic tissue

Karine Choquet, Jonathan Vappou, Paolo Cabras, Ounay Ishak, Afshin Gangi, Élodie Breton

## ► To cite this version:

Karine Choquet, Jonathan Vappou, Paolo Cabras, Ounay Ishak, Afshin Gangi, et al.. Magnetic Resonance Acoustic Radiation Force Imaging (MR-ARFI) for the monitoring of High Intensity Focused Ultrasound (HIFU) ablation in anisotropic tissue. *Magnetic Resonance Materials in Physics, Biology and Medicine*, 2023, 36, pp.737-747. 10.1007/s10334-023-01062-6 . hal-04126004

**HAL Id: hal-04126004**

**<https://hal.science/hal-04126004>**

Submitted on 20 Nov 2023

**HAL** is a multi-disciplinary open access archive for the deposit and dissemination of scientific research documents, whether they are published or not. The documents may come from teaching and research institutions in France or abroad, or from public or private research centers.

L'archive ouverte pluridisciplinaire **HAL**, est destinée au dépôt et à la diffusion de documents scientifiques de niveau recherche, publiés ou non, émanant des établissements d'enseignement et de recherche français ou étrangers, des laboratoires publics ou privés.

# **Magnetic Resonance Acoustic Radiation Force Imaging (MR-ARFI) for the monitoring of High Intensity Focused Ultrasound (HIFU) ablation in anisotropic tissue**

Karine Choquet<sup>1</sup>, Jonathan Vappou<sup>1</sup>, Paolo Cabras<sup>1,2</sup>, Ounay Ishak<sup>1</sup>, Afshin Gangi<sup>1,3</sup>, Elodie Breton<sup>1</sup>

<sup>1</sup>*Université de Strasbourg, CNRS, ICube, UMR 7357, Strasbourg, France.*

<sup>2</sup>*Image Guided Therapy, Pessac, France*

<sup>3</sup>*Department of interventional imaging, Hôpitaux Universitaires de Strasbourg, Strasbourg, France*

## **ABSTRACT**

**Object** We introduce a non-invasive MR-Acoustic Radiation Force Imaging (ARFI)-based elastography method that provides both the local shear modulus and temperature maps for the monitoring of High Intensity Focused Ultrasound (HIFU) therapy.

**Materials and Methods** To take tissue anisotropy into account, the local shear modulus  $\mu$  is determined in selected radial directions around the focal spot by fitting the phase profiles to a linear viscoelastic model, including tissue-specific mechanical relaxation time  $\tau$ . MR-ARFI was evaluated on a calibrated phantom, then applied to the monitoring of HIFU in a gel phantom, ex vivo and in vivo porcine muscle tissue, in parallel with MR-thermometry.

**Results** As expected, the shear modulus polar maps reflected the isotropy of phantoms and the anisotropy of muscle. In the HIFU monitoring experiments, both the shear modulus polar map and the thermometry map were updated with every pair of MR-ARFI phase images acquired with opposite MR-ARFI-encoding. The shear modulus was found to decrease (phantom and ex

vivo) or increase (in vivo) during heating, before remaining steady during the cooling phase. The mechanical relaxation time, estimated pre- and post-HIFU, was found to vary in muscle tissue.

**Discussion** MR-ARFI allowed for monitoring of viscoelasticity changes around the HIFU focal spot even in anisotropic muscle tissue.

## KEYWORDS

- Magnetic Resonance Guided Interventional Procedures
- High-Intensity Focused Ultrasound Ablation
- Acoustic Radiation Force Impulse Imaging
- Anisotropy
- Tissue Elasticity Imaging

## ACKNOWLEDGMENTS

This work has benefitted from funding of the FUI (Fonds Unique Interministériel, BPI France) for the UFOGUIDE project, and the ANR (Agence Nationale de la Recherche) French national program “Investissements d’Avenir” for the LABEX-CAMI (ANR-11-LABX-0004), the IHU Strasbourg (Institute of Image Guided Surgery, ANR-10-IAHU-0002) and the LabCom TechnoFUS lab (ANR-21-LCV3-0007-01).

## **Introduction**

High Intensity Focused Ultrasound (HIFU) thermal therapy is a non-ionizing and non-invasive clinical procedure that relies on localized absorption of the acoustic energy. To ensure the safety and efficiency of the therapy, it is usually performed either under magnetic resonance (MR) [1–3] or diagnostic ultrasound (US) imaging guidance [4]. Several non-invasive MR and US temperature monitoring methods have been proposed for estimating the temperature variation during HIFU ablation [5–9]. Among them, the Proton Resonance Frequency Shift (PRFS) MR technique [10, 11] is currently the clinical gold-standard [12] due to its tissue-independency over a wide temperature range. However, the limitations of PRFS MR-thermometry – such as its sensitivity to magnetic field variations and the presence of fat molecules – call for the development of complementary biomarkers.

In addition to temperature information, the alteration of mechanical properties related to actual thermal tissue damage have been investigated using elastography techniques [13–17]. Several MR Imaging (MRI)-based methods have been proposed to track biomechanical changes in tissues undergoing HIFU therapy. Using harmonic MR Elastography (MRE) [18], local irreversible increase in stiffness was reported as a result of HIFU ablation in *ex vivo* porcine muscle tissues [19]. It is worth noting that, PRFS temperature information may also be recovered simultaneously from MRE data using a gradient echo MR sequence [15, 20, 21]. Using real-time MRE and MR-thermometry, Kim et al. [20] reported a significant decrease in the shear modulus of *ex vivo* porcine muscle tissue as a consequence of moderate temperature elevation induced by HIFU. Nonetheless, MRE requires induction of shear waves with an external mechanical exciter that complexifies the interventional set-up, which is usually already bulky. For this reason, using the HIFU transducer as the source of both treatment and shear wave elastography waves represents a promising solution.

Due to absorption and scattering effects in biological tissues, HIFU pulses exert an acoustic radiation force, i.e. tissues locally undergo a micrometric displacement that causes the propagation of shear waves [22, 23]. Derived from the ultrasound Acoustic Radiation Force Impulse (ARFI) Imaging [24], the MR-ARFI imaging approach was proposed [25, 26], based on encoding the acoustic displacement in the MR phase signal using an appropriate motion-sensitive sequence. Originally, MR-ARFI consisted in generating a brief ultrasound wave train and then imaging this displacement to locate the focal spot or to correct for acoustic aberrations for HIFU therapy planning [27–29]. The use of ARFI has also been suggested to perform MR transient elastography [30], paving the way for monitoring HIFU ablations. As ARFI-induced tissue displacements are inversely correlated to the stiffness of the tissue, multiple papers described MR-ARFI displacement-based monitoring methods [31–36]. However, ARFI-induced displacements not only depend on the local tissue elasticity, but also on mechanical boundary conditions and tissue acoustic absorption, the latter parameters being susceptible to change during thermal ablations. To overcome this limitation, Vappou et al. [37] developed a method that relates MR-ARFI spot profile to tissue's local shear wave velocity and, by consequence, assuming a linear viscoelastic model, shear modulus during HIFU ablations. The paper reported an irreversible increase in tissue stiffness of *ex vivo* HIFU-ablated tissue, making it an interesting biomarker of thermal damage. However, the linear viscoelastic model relied on two strong hypotheses: 1- the viscoelastic relaxation time  $\tau$  was arbitrarily set from the literature, hence not tissue-specific, 2- the tissue was assumed to be isotropic, which may be inaccurate for several soft tissues such as muscle or kidney. Indeed, in such anisotropic media, shear waves generated for elastography purposes are likely to propagate with different velocities depending on their direction [38].

In this study, we propose an MR-ARFI-based method that provides both temperature maps and stiffness polar maps for the monitoring of HIFU therapy. The viscoelastic model takes the

tissue-specific  $\tau$  into account, and the geometric attenuation of the mechanical wave. A validation experiment is performed in a homogeneous phantom calibrated for elastography. The capability of the proposed approach to monitor a HIFU ablation is tested in a tissue-mimicking gel phantom as well as in ex vivo and in vivo swine muscle tissue.

**Materials and Methods**

MR-ARFI for HIFU ablation monitoring

Following the principle of MR-ARFI first proposed by McDannold and Maier [26], the HIFU transducer delivering the HIFU therapy is also used to generate the ARFI mechanical wave within the tissue to be monitored. For that purpose, a short sonication pulse of the order of one millisecond is applied. This generates an acoustic radiation force which induces a micrometric displacement (push) in the focal zone (**Fig. 1a**), resulting in the propagation of a transient shear wave of velocity  $c_s$ . This mechanical wave is encoded on the MRI phase signal using bipolar motion sensitizing gradients (MSG) synchronized to the acoustic radiation force (**Fig. 1b**).

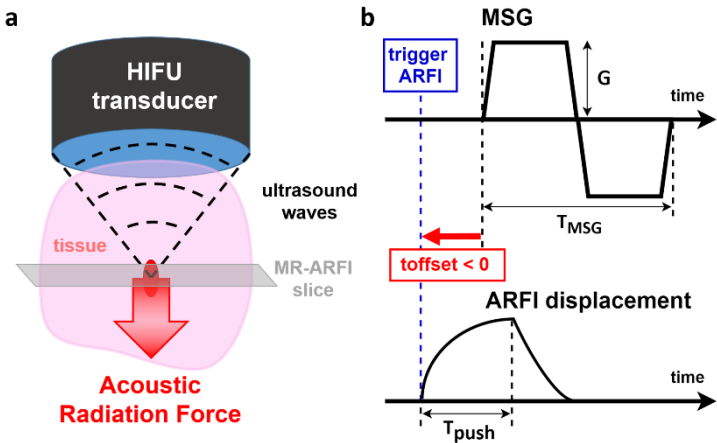


**Fig. 1** General concepts of MR-ARFI

**a:** The acoustic radiation force causes a shear wave to propagate through the tissue, away from the focal spot **b:** Chronogram and synchronisation between MSG and ARFI displacement

The resulting MR-ARFI phase profile (**Fig. 2, top left**) depends on tissue stiffness and viscosity. In general, stiffer tissues lead to a wider ARFI spot.

Vappou et al. [37] proposed to identify the experimental MR-ARFI phase profile to a theoretical one, allowing determination of  $c_s$  and therefore the local shear modulus  $\mu$  at the focal spot, assuming that the medium is isotropic, linear viscoelastic and locally homogeneous of density  $\rho \approx 1000 \text{ kg / m}^3$ :

$$\mu = \rho c_s^2 \quad \text{Equation 1}$$

The theoretical MR-ARFI profile in the phase image is given by:

$$\phi_{th}(r, \theta) = \gamma \int_0^{T_{MSG}} G(t) \delta(r, \theta, t) dt \quad \text{Equation 2}$$

where  $\gamma$  is the gyromagnetic ratio of the hydrogen nucleus,  $G$  is the MSG amplitude,  $T_{MSG}$  its duration, and  $\delta(r, \theta, t)$  is the displacement at time  $t$  written in polar coordinates  $(r, \theta)$  (**Fig. 2**). To

model tissue viscoelasticity,  $\delta$  at the focal spot ( $r = 0$ ) is assumed to follow a 1<sup>st</sup> order exponential law of time constant  $\tau$  representing the mechanical relaxation time of the tissue:

$$\delta(\mathbf{r} = \mathbf{0}, \theta, t) = \begin{cases} \mathbf{0} \leq t \leq T_{push} : \delta(t) = D \left( \mathbf{1} - e^{-\frac{t}{\tau}} \right) \\ t \geq T_{push} : \delta(t) = D \left( \mathbf{1} - e^{-\frac{T_{push}}{\tau}} \right) e^{-\frac{t - T_{push}}{\tau}} \end{cases} \quad \text{Equation 3}$$

where  $\tau$  is the mechanical relaxation time of the tissue,  $T_{push}$  corresponds to the duration of the ARFI push and  $D$  to the asymptotic value of the ARFI displacement at the focal spot. The ARFI displacement induced away from the focal spot is described along radial propagation lines ( $r > 0$  at a given  $\theta$  angle) considering the medium as locally homogeneous:

$$\delta(r, \theta, t) = \begin{cases} t < \frac{r}{c_s} : \delta(t) = 0 \\ t \geq \frac{r}{c_s} : \delta(t) = \frac{1}{\sqrt{r}} \delta\left(0, \theta, t - \frac{r}{c_s}\right) \end{cases} \quad \text{Equation 4}$$

with  $c_s$  denoting the shear wave velocity. Hence, the propagation of the shear wave is modeled as a rectilinear translation along 1D radial lines of the displacement  $\delta(r = 0, \theta, t)$  induced at the focal point (**Fig. 2**), where  $\frac{r}{c_s}$  is the time delay corresponding to the arrival of the wavefront at position  $r$ . Assuming a cylindrically-shaped wavefront, the attenuation in amplitude is modeled as inversely proportional to the square root of the distance ( $r$ ) from the excitation source.

#### Anisotropic MR-ARFI for HIFU ablation monitoring

In this paper, the approach is further developed to estimate tissue anisotropy around the focal spot. The shear modulus  $\mu$  is computed in predetermined radial directions around the focal spot, by individually fitting 1D radial phase profiles to the linear viscoelastic model assuming that the medium is locally homogeneous along each radial direction (**Fig. 2**).

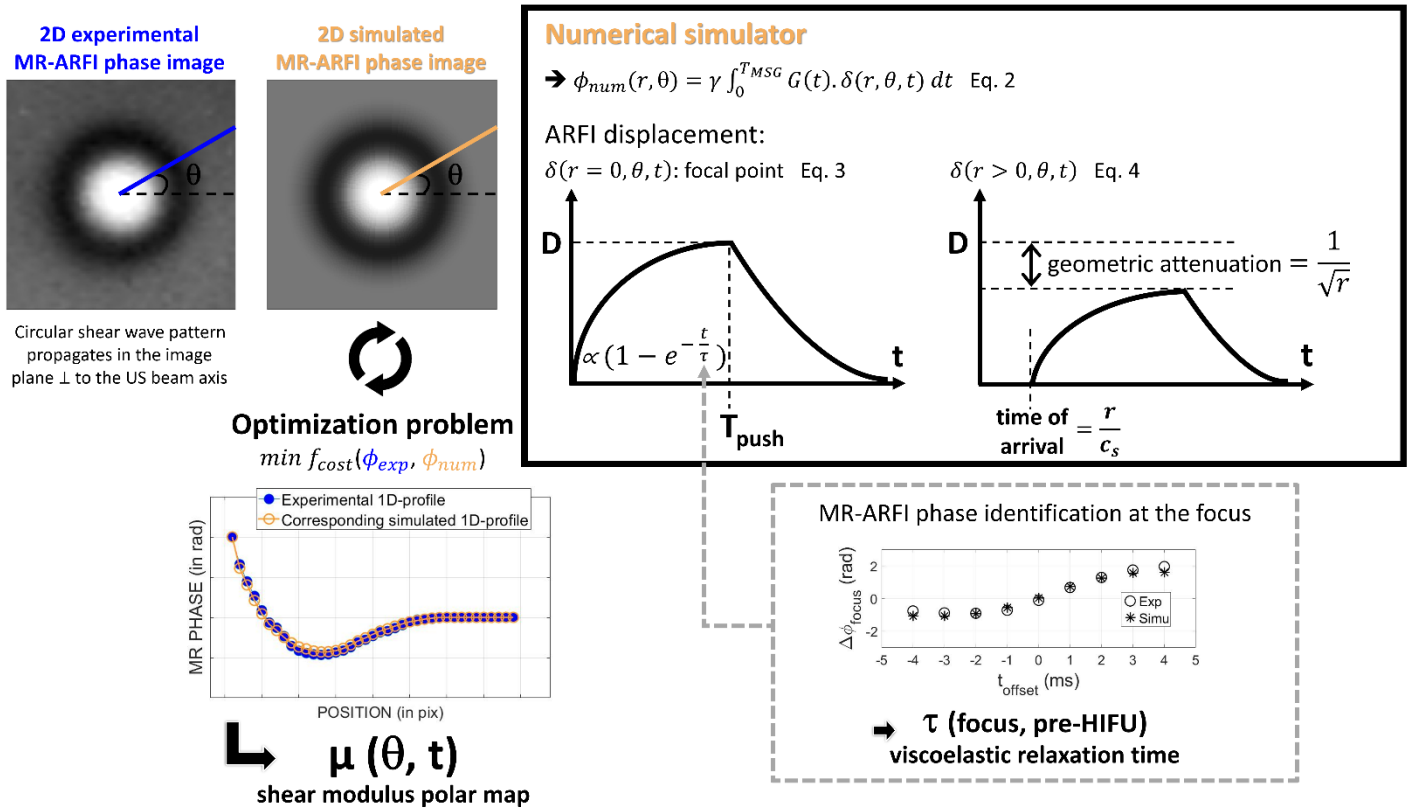


**Fig. 2 Identification process of the viscoelastic properties using the proposed MR-ARFI-based method illustrated in a homogeneous medium**

Experimental radial 1D ARFI profiles are individually fitted to theoretical ones (bottom left) generated by a numerical simulator (right), relying on a viscoelastic shear wave propagation model with geometric attenuation. The viscoelastic relaxation time  $\tau$  used in the model is determined experimentally once before the HIFU treatment at the focal spot.

The specific relaxation time  $\tau$  of the tissue at the focal spot is determined experimentally prior to the HIFU treatment following the approach published by Kaye et al. [39] and Dadakova et al. [40]. For that purpose, several MR-ARFI images are acquired with different time shift  $t_{\text{offset}}$  values (**Fig. 1b**), and the MR phase signal measured in the central pixel of the focal spot is fitted (**Fig. 2, bottom right**) according to **Equation 2** and **3**.

The experimental MR-ARFI images were resampled using linear spatial interpolation by a factor of two for the identification process. Background voxels are first masked out based on their magnitude. Hence, the radial 1D phase profiles centered on the focal spot are extracted from the masked spatially interpolated MR-ARFI phase image. A bounded optimization algorithm [41] is used to maximize the correlation between the experimental and simulated 1D MR phase profiles. The solution domain is constrained according to realistic physical limits, namely  $0.8 \text{ kPa} \leq \mu \leq 100 \text{ kPa}$  for the shear modulus [19, 42].

### MR-ARFI experiments

Two different series of experiments were planned. The first experiments aimed at evaluating the accuracy and quantitative nature of the proposed method for elastography on a calibrated phantom. Then, the ability of the proposed method to monitor HIFU heating in different scenarios (phantom, ex-vivo and in-vivo) was evaluated.

The same MR pulse sequence was used for all experiments: a segmented echo planar imaging (EPI) gradient echo sequence with MSG and focused ultrasound (FUS) trigger adjuncts was developed. The  $t_{\text{offset}}$  parameter is used to trigger the ARFI push relatively to the beginning of the MSG (**Fig. 1b**). Experiments were performed on 1.5 T MRI systems (MAGNETOM Aera and MAGNETOM Sola, Siemens Healthineers, Germany). Main acquisition parameters were: TR 500 ms, TE 28 ms, FOV 256 mm  $\times$  256 mm (320 mm  $\times$  320 mm for the in vivo experiment), matrix 128  $\times$  128, slice thickness 5 mm (6 mm for the in vivo experiment), EPI factor 37, MSG:

G 36 mT/m -  $T_{\text{MSG}}$  10 ms - slice encoding direction. The spine coil was used in all the experiments. To improve the SNR, it was combined alternatively with a 19-cm flexible loop coil for both phantom experiments, or with the body matrix coil for the in vivo experiment.

At every time step, two MR-ARFI images are sequentially acquired with opposite MSG polarity. This feature has two advantages: (1) it allows doubling the displacement sensitivity in MR-ARFI, by performing the difference between the two phase images and (2) it allows retrieving simultaneously temperature maps through proton resonance frequency shift (PRFS) thermometry by averaging the two phase images [15, 21]. PRFS with  $B_0$ -drift correction is used to measure temperature changes. Phase difference images were spatially unwrapped for elastography, while average phase images were temporally unwrapped for thermometry.

Assuming the shear wave propagates perpendicularly to the US beam axis, the MSG direction was set parallel to this axis to encode axial tissue displacement, and the acquisition slice was positioned perpendicular to this axis (**Fig. 1a**). A 1 MHz 128-element spherical transducer (Imasonic, France) with a nominal focal length of 6 cm was used for all the experiments, for both ARFI push and therapy. The transducer was driven by an MR-compatible, 256-channel HIFU generator (Image Guided Therapy, Pessac, France). A latex balloon filled with degassed water was used for acoustic coupling. A granular jamming positioning system held the transducer in place during all experiments [43]. The ARFI push duration was set equal to  $T_{\text{MSG}}/2 = 5$  ms.

The quantitative nature of the proposed method was first evaluated in a homogeneous commercial phantom calibrated for elastography (CIRS, Norfolk, USA). The value of reference provided by the manufacturer for shear elastic modulus is  $5.9 \text{ kPa} \pm 5\%$ . The acoustic power of the ARFI shots was set to 200 W. The delay  $t_{\text{offset}}$  between the ARFI push and the MSG was

varied from -6 to 1 ms, every 1 ms, these measures being repeated 4 times. These data were used to estimate the viscoelastic relaxation time  $\tau$  at the focus, and to study the sensitivity of the local radial shear modulus  $\mu$  to  $t_{\text{offset}}$ .

HIFU heating was then monitored using the proposed method. It was first evaluated in a tissue-mimicking phantom, made of porcine gelatin powder (160 g), water (2.6 kg) and condensed milk (800 g) containing 8 % fat and 55% sugar in order to increase the acoustic absorption [42]. Before refrigeration, the mixture was degassed using a vacuum chamber.

For the ex-vivo experiment, a porcine muscle was obtained from local butcher, whereas the in-vivo tests were performed on one swine model (male, 32 kg). The pig was anesthetized (1.8% isoflurane) and placed supine with the HIFU transducer positioned on its right thigh.

The FUS sequence consisted in interleaving a HIFU heating phase with an ARFI shooting phase within each TR period (**Fig. 3**).

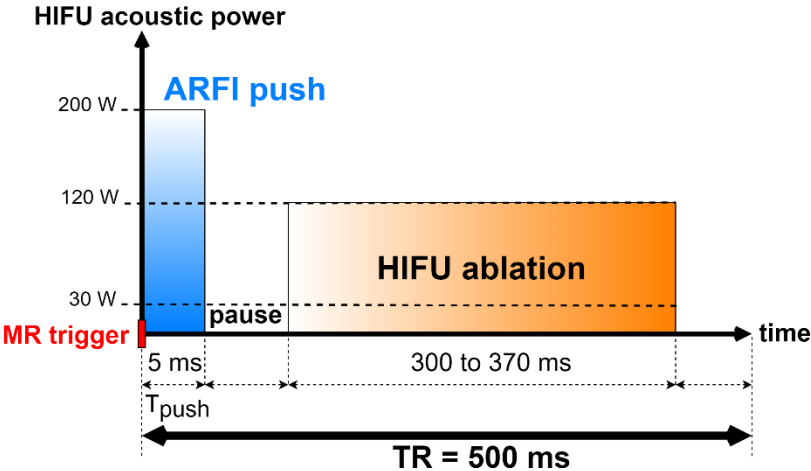


**Fig. 3 FUS sequence for the monitoring experiments** (note that a qualitative time scale is used here for readability reasons)

HIFU and ARFI sequence parameters are provided in **Table 1**. The  $t_{\text{offset}}$  parameter was manually chosen for each experiment according to the extent of the MR-ARFI pattern for the given  $T_{\text{push}}/T_{\text{MSG}}$  configuration.

	Phantom experiment	Ex vivo experiment	In vivo experiment
ARFI $t_{\text{offset}}$	-2 ms	1 ms	-3 ms
TR	500 ms		
ARFI shots	$T_{\text{push}}$ 5 ms (duty cycle 1%) 200 W acoustic power		
Pause	70 ms	50 ms	50 ms
HIFU heating	$T_{\text{heating}}$ 370 ms (duty cycle 74%) 30 W acoustic power	$T_{\text{heating}}$ 300 ms (duty cycle 60%) 80 W acoustic power	$T_{\text{heating}}$ 300 ms (duty cycle 60%) 120 W acoustic power

**Table 1.** HIFU and ARFI sequence parameters

Polar maps of the shear modulus  $\mu(\theta)$  were drawn for 64 angles equally distributed in the interval  $\theta \in [0^\circ: 360^\circ]$ .

Prior and after each HIFU experiment, the phantom/tissue mechanical relaxation time  $\tau$  was determined with  $t_{\text{offset}}$  varying from -5 ms to 4 ms every 1 ms, -2.5 ms to 2 ms every 0.5 ms, and -5 ms to 0.5 ms every 0.5 ms, for the gelatin phantom, ex vivo and in vivo muscle experiments, respectively.

## Results

### Calibrated phantom experiment

The value of reference determined for  $\tau$  is 3.4 ms at the focal spot. MR-ARFI phase profiles acquired with 4 increasing values of  $t_{\text{offset}}$  can be seen from left to right in **Fig. 4** (top row). Corresponding  $\mu$  polar maps averaged over the 4 repetitions are displayed on the bottom row.

All phase profiles and  $\mu$  polar maps can be found in a separate figure (Online Resource 1). The obtained polar representations of  $\mu$  appear circular, characteristic of an isotropic medium.

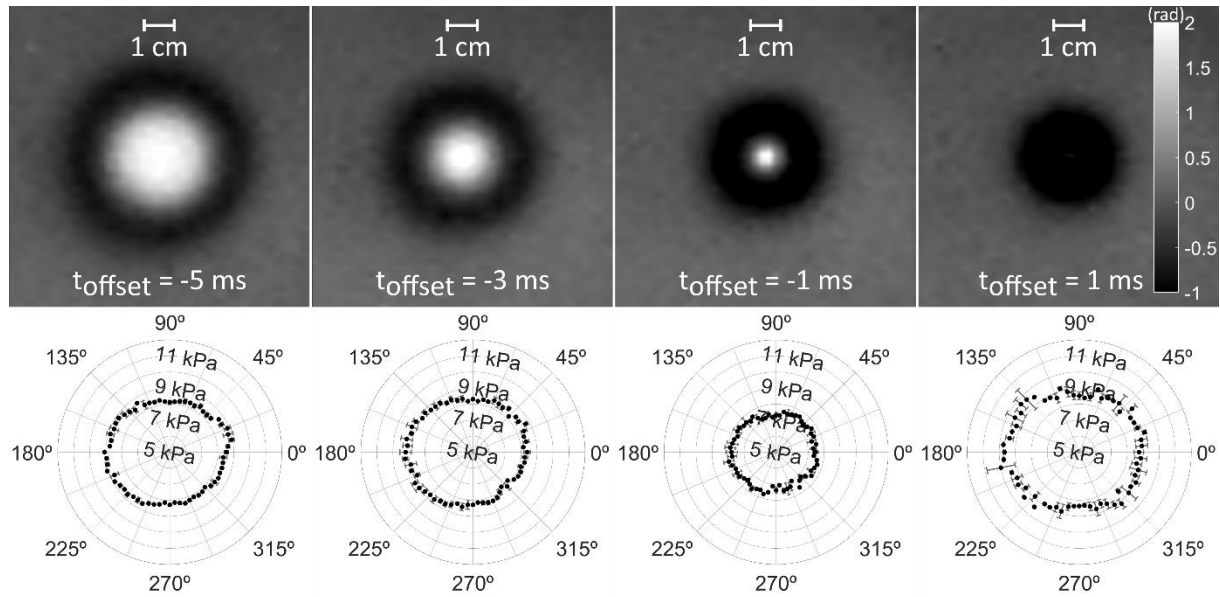


**Fig. 4 Calibrated phantom experiment**

(Top row) 2D MR-ARFI spots acquired during the 2<sup>nd</sup> repetition for 4 increasing values of  $t_{\text{offset}}$

(Bottom row) Associated  $\mu(\theta)$  polar maps representing the average (black circle) and standard deviation (error bar) over the 4 repetitions. Note that the scale of the polar maps is 5 kPa (center) to 12 kPa (outer circle).

Assuming strict isotropy, the average and standard deviation of  $\mu$  across all directions  $\theta$  and 4 repetitions for each  $t_{\text{offset}}$  are given in **Table 2**. The average across all directions  $\theta$ , repetitions and  $t_{\text{offset}}$  is equal to  $8.2 \text{ kPa} \pm 7 \%$  for  $\mu$ .

$t_{\text{offset}}$	-6 ms	-5 ms	-4 ms	-3 ms	-2 ms	-1 ms	0 ms	1 ms
Rep. 1	$8.0 \pm 0.2$	$8.4 \pm 0.3$	$8.7 \pm 0.3$	$8.5 \pm 0.4$	$7.8 \pm 0.3$	$7.5 \pm 0.2$	$8.0 \pm 0.3$	$9.0 \pm 0.4$
Rep. 2	$8.0 \pm 0.2$	$8.5 \pm 0.3$	$8.7 \pm 0.3$	$8.5 \pm 0.4$	$7.8 \pm 0.3$	$7.5 \pm 0.2$	$7.9 \pm 0.3$	$9.1 \pm 0.4$
Rep. 3	$8.0 \pm 0.3$	$8.5 \pm 0.3$	$8.8 \pm 0.4$	$8.5 \pm 0.4$	$7.9 \pm 0.3$	$7.5 \pm 0.3$	$7.8 \pm 0.4$	$8.9 \pm 0.5$
Rep. 4	$8.0 \pm 0.2$	$8.5 \pm 0.3$	$8.8 \pm 0.4$	$8.5 \pm 0.5$	$7.8 \pm 0.4$	$7.5 \pm 0.3$	$7.8 \pm 0.3$	$8.9 \pm 0.6$
Global average (kPa)	$8.0 \pm 0.2$	$8.5 \pm 0.3$	$8.8 \pm 0.3$	$8.5 \pm 0.4$	$7.8 \pm 0.3$	$7.5 \pm 0.3$	$7.9 \pm 0.3$	$9.0 \pm 0.5$

**Table 2.** Mean  $\pm$  standard deviation for each  $t_{\text{offset}}$  of the shear modulus (kPa) found with MR-ARFI in the commercial phantom, assuming isotropy (average over all radial directions), for each of the 4 repetitions and global values over the 4 repetitions

### MR-ARFI monitoring experiments

For each experiment, the acquisition time for both temperature and  $\mu$  polar maps was 4 s, corresponding to the acquisition of 2 MR images with opposite motion sensitivity polarities.

### Tissue-mimicking phantom

During the HIFU ablation in the gelatin phantom, the MR-ARFI spot diameter was observed to decrease versus time as shown in the video (Online Resource 2), suggesting that the gel softens as a result of heating. This can be observed from the  $\mu$  polar maps obtained pre- and post-ablation (**Fig. 5**), their circular shape reflecting the high isotropy of the phantom. The shear modulus  $\mu$  was found to decrease from around 5 kPa to 3 kPa, while temperature increased by 12°C at the central pixel of the focal spot (**Fig. 5**). Regarding  $\tau$ , its value was found constant pre- and post-HIFU at 5.2 ms.

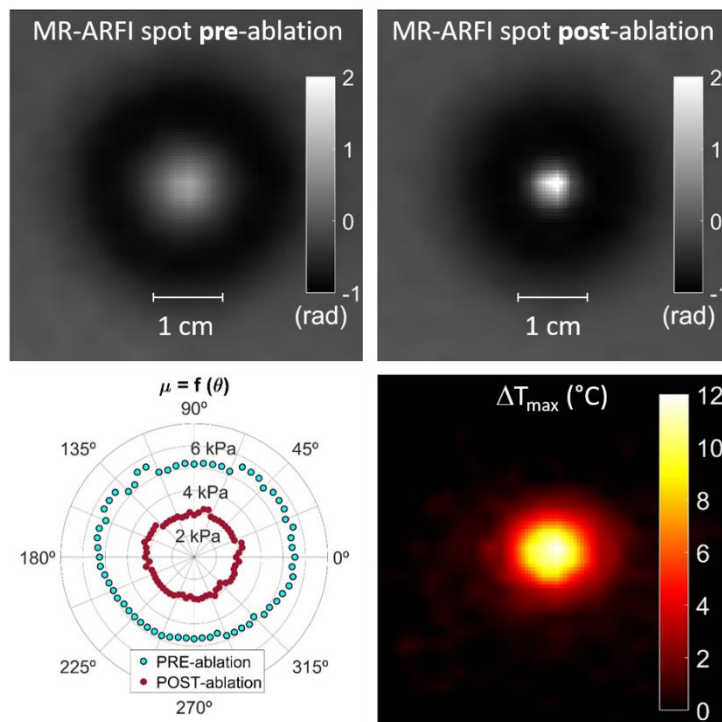


**Fig. 5** HIFU ablation in a gelatin phantom

MR-ARFI images acquired before and after the HIFU heating (top row) and corresponding  $\mu(\theta)$  polar maps (bottom left). Temperature variation map obtained at the end of HIFU heating (bottom right). The spatial resolution ( $\Delta x = 0.5 \text{ mm}$ ) and size ( $50.8 \text{ mm} \times 50.8 \text{ mm}$ ) of displayed temperature map region were matched to those of the displayed interpolated MR-ARFI spots.

Ex vivo tissue

In the ex vivo porcine tissue experiment, the muscle tissue appeared to be highly anisotropic, as depicted by the oval MR-ARFI spots and the resulting peanut-shaped  $\mu$  polar maps shown in **Fig. 6** before and after HIFU.  $\tau$  increased slightly from 2.2 ms pre-heating to 2.6 ms post-heating, while  $\mu$  globally decreased during HIFU heating (video Online Resource 3). In this HIFU experiment, the temperature increased by  $22^\circ\text{C}$  at the central pixel of the focal spot.

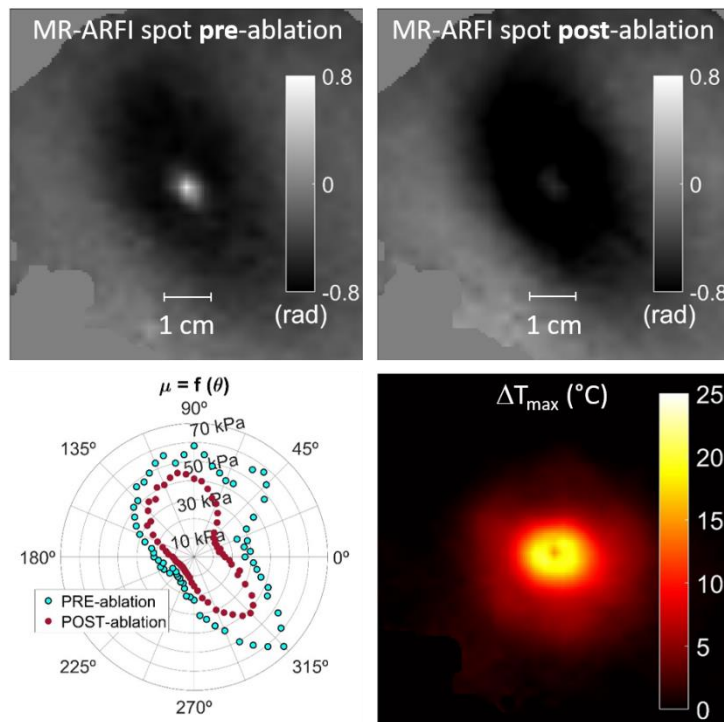


**Fig. 6** HIFU ablation in ex vivo porcine muscle

MR-ARFI images acquired before and after the HIFU heating (top row) and corresponding  $\mu(\theta)$  polar maps (bottom left). Temperature variation map obtained at the end of HIFU heating (bottom right). The spatial resolution ( $\Delta x = 0.5$  mm) and size ( $76$  mm  $\times$   $76$  mm) of displayed temperature map region were matched to those of the displayed interpolated MR-ARFI spots.

### In vivo tissue

In porcine muscle in vivo, the MR-ARFI spot was observed to widen progressively with time (video Online Resource 4), which is consistent with the increase in shear modulus  $\mu(\theta)$  observed in the polar plots during the ablation.  $\tau$  was found to increase as well, from 5.8 ms pre-ablation to 13.9 ms post-ablation. The maximum temperature rise reached at the focus was 50 °C. Looking at the MR-ARFI phase profiles, one can notice that the images are obscured by an oblique band of phase wrapping-related artifacts. As it was poorly corrected by unwrapping, we excluded this area from the identification process. **Fig. 7** then shows the shear modulus angular distribution estimated in the left half of the MR-ARFI spot, both pre- and post-heating in tissues that appeared to be anisotropic.

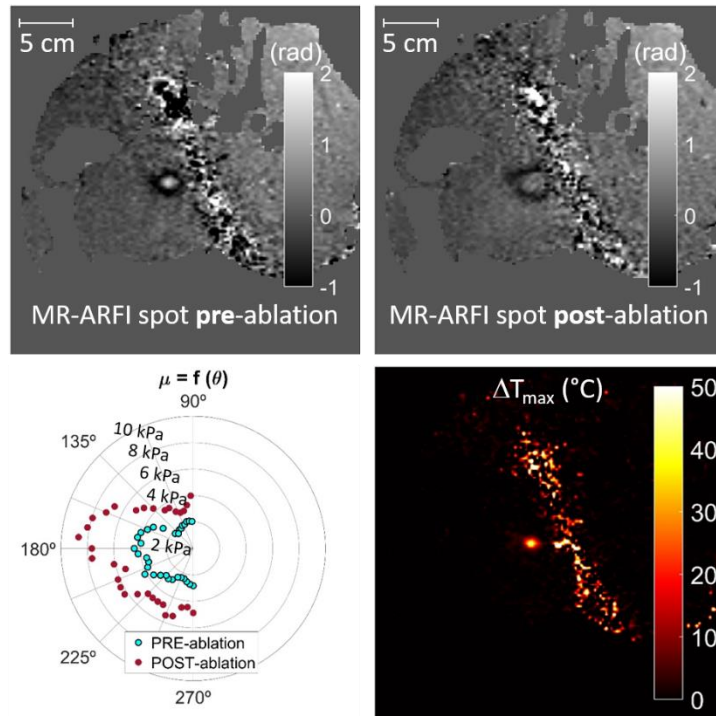


**Fig. 7 In vivo HIFU ablation**

MR-ARFI images acquired before and after the HIFU heating (top row) and corresponding  $\mu(\theta)$  polar maps (bottom left). Temperature variation map obtained at the end of HIFU heating (bottom right). The spatial resolution ( $\Delta x = 0.6$  mm) and size ( $320$  mm  $\times$   $320$  mm) of displayed temperature map region were matched to those of the displayed interpolated MR-ARFI spots. Due to the presence of an oblique band of phase wrap,  $\mu(\theta)$  polar maps were estimated for the left half of the ARFI spot, i.e.  $\theta$  from  $90^\circ$  to  $270^\circ$ .

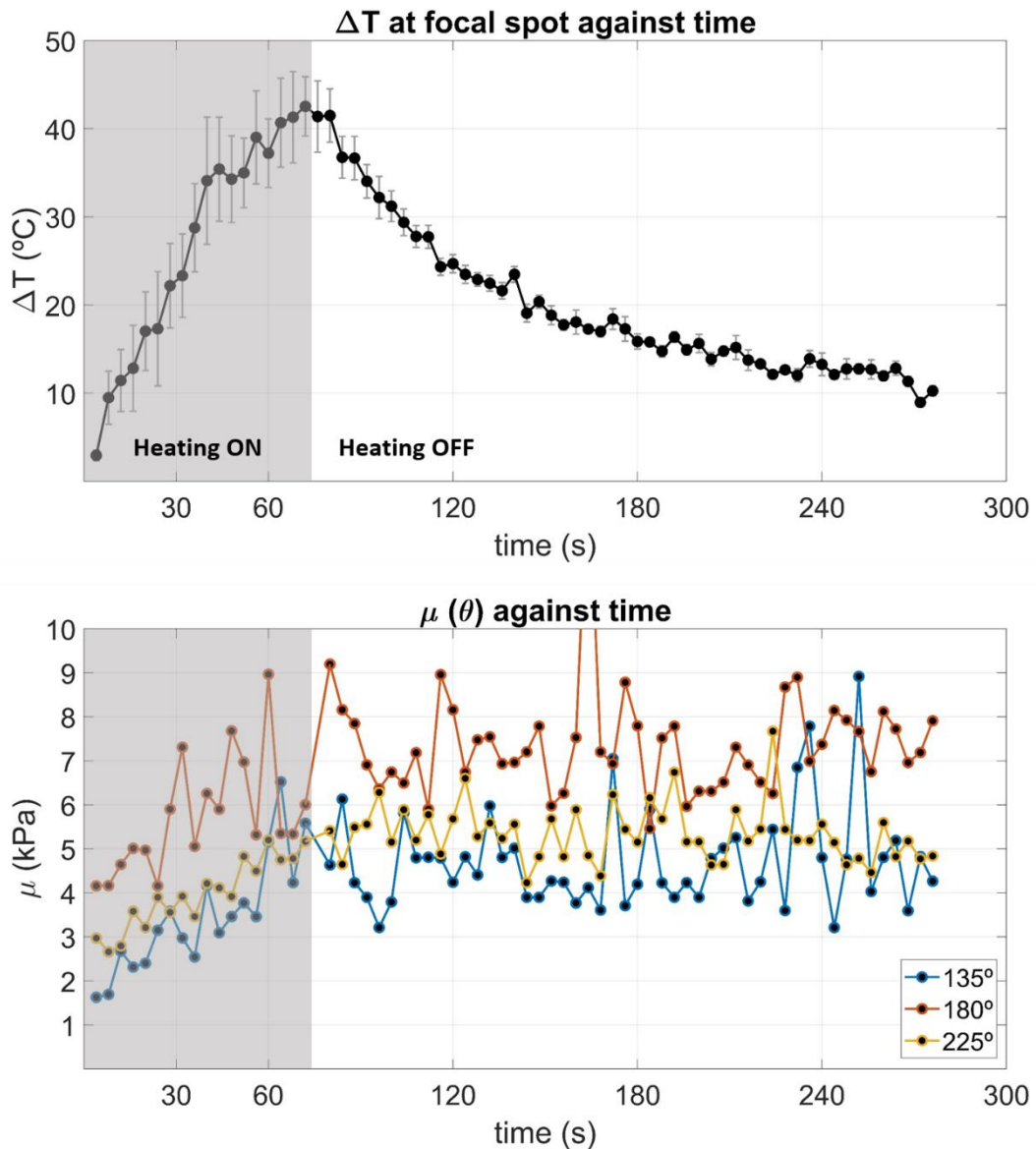


**Fig. 8 Temporal evolution of the temperature and shear modulus  $\mu(\theta)$  at the focal spot during the in vivo HIFU experiment**

(Top) Temperature changes during the in vivo HIFU experiment in porcine muscle are estimated through MR-PRFS in a circular focus-centered region of interest 5.4 mm in diameter. (Bottom) The temporal evolution of the radial shear modulus around the focal spot is given for 3 representative radii with  $\theta$  angle 135°, 180° and 225° as shown **Fig. 7**.

## Discussion

In this paper, we introduce a method that provides both shear modulus polar maps and temperature maps for the monitoring of HIFU therapy. The present MR-ARFI shear wave velocity-based approach allows for the characterization of tissue anisotropy while taking into account the viscoelastic relaxation time  $\tau$  determined before the ablation. Concurrent monitoring and therapy were performed by interleaving short ARFI shots and HIFU heating at the focus during the HIFU treatment. The direction-dependant shear modulus  $\mu$  is then identified for a user-determined number of 1D MR-ARFI phase profiles centered on the HIFU focus, the result of the identification process being represented in a shear modulus polar map updated during the treatment.

In the commercial elasticity phantom, good repeatability was found between the 4 repetitions and all the polar maps radii of MR-ARFI for each individual  $t_{\text{offset}}$ . The profile of the shear modulus polar map was consistent with the expected isotropy of the phantom. Although the shear modulus determined with MR-ARFI ( $8.2 \text{ kPa} \pm 7 \%$ ) was in the same range as the one reported by the manufacturer ( $5.9 \text{ kPa} \pm 5 \%$ ), there was a significant difference that may be due to differences between mechanical testing protocols. Indeed, the value provided by the manufacturer has been obtained through mechanical indentation whereas our approach is based on the propagation of a transient shear wave. It is well known that quasi-static and dynamic elastography methods may yield different results due to the differences in excitation frequencies [44, 45].

Our results highlight the influence of the  $t_{\text{offset}}$  parameter on the shear modulus identification process. This parameter allows for controlling the size of the MR-ARFI pattern for a given  $T_{\text{push}}/T_{\text{MSG}}$  configuration. On the one hand, a small ARFI spot - compared to the spatial resolution of the image - can lead to errors in the fitting process due to the limited amount of

data available in the radial phase profile. On the other hand, a large ARFI spot is more sensitive to the hypothesis of local homogeneity of the shear modulus along each propagation radius. In addition, a large focal spot may be particularly sensitive to shear wave dispersion effects that are not taken into account in the current model, as the displacement profile is assumed to be unchanged in shape during propagation (**Fig. 2** and **Eq.4**). These extreme values of  $t_{\text{offset}}$  may result in significant errors in shear modulus estimates, as a result of inaccuracy of the MR-ARFI phase identification process. For these reasons, an optimal value for  $t_{\text{offset}}$  should be carefully chosen before each monitoring experiment, in order to control the size of the initial MR-ARFI spot.

Resulting from the identification process of each individual radial phase profile of the ARFI spot, the polar maps obtained with MR-ARFI reflected the isotropy of gel phantoms, and the anisotropy of biological soft tissue as observed in ex vivo and in vivo porcine muscle. It should be noted that the number and values of  $\theta$  angles shown in the polar map can be freely defined, taking the spatial resolution and the computation time into account. During HIFU treatment, the polar maps obtained with MR-ARFI mainly reflect the intrinsic anisotropy of the tissue. They may also help in detecting direction-dependent changes in tissue elasticity during the HIFU treatment, as a result of vascular perfusion for instance. The current model proposes an increment towards the characterization of anisotropic tissues; however, it relies on the strong hypothesis that the medium is radially homogeneous within the ARFI-spot. This hypothesis may be particularly inaccurate in tissues featuring curved muscle fibers, such as the heart.

The decrease of the shear modulus observed during HIFU in the gelatin phantom reflects the gel softening due to HIFU heating. Ex vivo porcine muscle tissue was observed to soften, as already reported in the literature [19, 20, 46] with moderate temperature increase. The in vivo HIFU ablation in porcine thigh muscle resulted in local tissue stiffening as expected for higher temperature elevations [13, 19, 37, 47].

Other MR-ARFI-based elastography approaches have been recently introduced. With the combination of multiple ARFI pushes in a plane perpendicular to the ultrasound propagation axis, Hofstetter et al.'s time of flight-based approach [48, 49] can provide an extended spatial mapping of elasticity. Another study, based on the generation of a “supersonic” series of ARFI pushes on a line, aimed at mapping tissue mechanical properties in a plane parallel to the ultrasound axis [50]. Both methods rely on the resolution of a complex inverse problem and the use of algorithms to estimate the shear wave velocity with several wave-propagation time steps. In comparison, our method has been adapted for local estimation of viscoelasticity only within the HIFU ablation area i.e. directly where the ARFI push is applied. Although it does not allow for spatial mapping of the mechanical properties, our approach combines several advantages, such as the requirement of only one wave-propagation time step during the monitoring, which renders it particularly interesting in terms of temporal resolution, and the possibility to take tissue viscoelasticity into account through the evaluation of the  $\tau$  parameter. Under the assumption of a linear viscoelastic model, this time constant is considered as an intrinsic property of the tissue, equal to the ratio between dynamic viscosity  $\eta$  and shear modulus  $\mu$ . As a consequence, the value of  $\tau$  is the same for both loading (ultrasound push ON) and relaxation (ultrasound OFF) phases, as already modelled in prior work [30].

A major limitation of our model is that it does not consider shear wave dispersion, despite the fact that tissue is assumed to exhibit a viscoelastic response. The transient ARFI excitation leads to the propagation of shear waves with a given frequency content that was not considered in our model. Indeed, the shear wave propagation was modelled as a simple temporal shift of the focal displacement (**Eq. 3-4**). The major effect of this approximation is that our model ignores the distortion of the temporal displacement profile as it travels away from the focus, since it is assumed to always follow a strict first order exponential behavior (**Eq. 3-4**). An important

improvement would be to refine the shear wave propagation model, by using for instance simulations based on Green's functions [51] in order to take shear wave dispersion into account.

One of the major side findings of this study is that both the viscoelastic mechanical relaxation time  $\tau$  and the dynamic viscosity  $\eta$ , defined as  $\eta = \tau \cdot \mu$ , were found to vary during the ablation in both ex vivo and in vivo porcine muscle. Although this is a promising finding, since it suggests that viscoelastic parameters may also serve as biomarkers of tissue integrity, it represents a significant limit to our method, which assumes that  $\tau$  is steady during the ablation. Identifying both  $\tau$  and  $\mu$  at the same time during the ablation seems therefore a necessary improvement to the proposed method. However, it may lead to much longer acquisitions, thus not compatible with the real-time requirements of HIFU ablation monitoring. Indeed, the current MR-ARFI-based method for estimating  $\tau$  relies on the use of numerous acquisitions with different  $t_{\text{offset}}$  values [39, 40]. From an optimization point of view, fitting these 2 parameters remains challenging on a single 1D- MR-ARFI phase profile, given the limited spatial resolution and experimental phase-to-noise ratio of the MR images. For this purpose, re-shaping the identification process should be considered, which is beyond the scope of this paper.

In conclusion, a fast, non-invasive method has been proposed for the monitoring of tissue shear modulus and temperature during HIFU ablations. It provides quantitative shear modulus polar maps with every pair of MR-ARFI phase images acquired with opposite MR-ARFI-encoding. This fast local elasticity characterisation approach allows for monitoring tissue anisotropy, as illustrated in a tissue-mimicking gel phantom and in ex vivo and in vivo muscle porcine model.

### **Compliance with ethical standards**

The in vivo experiment was led following the 3R principle for more humane research, and in following local legal ethics regulation (registered project APAFIS #14092-2018031513247711

v1). The animal was maintained under gaseous anaesthesia during imaging (1.8% isoflurane), with appropriate pain management (Propofol 1mg/kg) during HIFU. At the end of the experiment, the animal was euthanized through anaesthetics overdose (10 min, 5% isoflurane) coupled to IV injection of saturated KCl solution (0.5 mL/kg).

## References

1. Jolesz FA (2009) MRI-Guided Focused Ultrasound Surgery. *Annu Rev Med* 60:417–430.
2. Kim Y (2015) Advances in MR image-guided high-intensity focused ultrasound therapy. *Int J Hyperthermia* 31:225–232.
3. Kuroda K (2018) MR techniques for guiding high-intensity focused ultrasound (HIFU) treatments. *J Magn Reson Imaging* 47:316–331.
4. Ebbini ES, Ter Haar G (2015) Ultrasound-guided therapeutic focused ultrasound: Current status and future directions. *Int J Hyperthermia* 31:77–89.
5. Ebbini ES, Simon C, Liu D (2018) Real-time Ultrasound Thermography and Thermometry. *IEEE Signal Process Mag* 35:166–174.
6. Geoghegan R, Haar G ter, Nightingale K, Marks L, Natarajan S (2021) Methods of monitoring thermal ablation of soft tissue tumors – a comprehensive review. *Med Phys* 49:769–791.
7. Lewis MA, Staruch RM, Chopra R (2015) Thermometry and ablation monitoring with ultrasound. *Int J Hyperthermia* 31:163–181.
8. Odéen H, Parker DL (2019) Magnetic resonance thermometry and its biological applications - Physical principles and practical considerations. *Prog Nucl Magn Reson Spectrosc* 110:34–61.
9. Rieke V, Pauly KB (2008) MR Thermometry. *J Magn Reson Imaging* 27:376–390.
10. De Poorter J (1995) Noninvasive MRI thermometry with the proton resonance frequency method: study of susceptibility effects. *Magn Reson Med* 34:359–367.
11. Ishihara Y, Calderon A, Watanabe H, Okamoto K, Suzuki Y, Kuroda K, Suzuki Y (1995) A precise and fast temperature mapping using water proton chemical shift. *Magn Reson Med* 34:814–823.
12. Kokuryo D, Kumamoto E, Kuroda K (2020) Recent technological advancements in thermometry. *Advanced Drug Delivery Reviews* 163–164:19–39.

13. Arnal B, Pernot M, Tanter M (2011) Monitoring of thermal therapy based on shear modulus changes: II. Shear wave imaging of thermal lesions. *IEEE Trans Ultrason Ferroelectr Freq Control* 58:1603–1611.
14. Chen J, Woodrum DA, Glaser KJ, Murphy MC, Gorny K, Ehman R (2014) Assessment of in vivo laser ablation using MR elastography with an inertial driver. *Magn Reson Med* 72:59–67.
15. Corbin N, Vappou J, Breton E, Boehler Q, Barbé L, Renaud P, de Mathelin M (2016) Interventional MR elastography for MRI-guided percutaneous procedures: Interventional MR Elastography. *Magn Reson Med* 75:1110–1118.
16. Mariani A, Kwiecinski W, Pernot M, Balvay D, Tanter M, Clement O, Cuenod CA, Zinzindohoue F (2014) Real time shear waves elastography monitoring of thermal ablation: in vivo evaluation in pig livers. *J Surg Res* 188:37–43.
17. Sapin-de Brosses E, Pernot M, Tanter M (2011) The link between tissue elasticity and thermal dose in vivo. *Phys Med Biol* 56:7755–7765.
18. Muthupillai R, Lomas DJ, Rossman PJ, Greenleaf JF, Manduca A, Ehman RL (1995) Magnetic resonance elastography by direct visualization of propagating acoustic strain waves. *Science* 269:1854–1857.
19. Wu T, Felmlee JP, Greenleaf JF, Riederer SJ, Ehman RL (2001) Assessment of thermal tissue ablation with MR elastography. *Magn Reson Med* 45:80–87.
20. Kim K, Breton E, Gangi A, Vappou J (2020) Simultaneous fat-referenced proton resonance frequency shift thermometry and MR elastography for the monitoring of thermal ablations. *Magn Reson Med* 84:339–347.
21. Le Y, Glaser K, Rouviere O, Ehman R, Felmlee JP (2006) Feasibility of simultaneous temperature and tissue stiffness detection by MRE. *Magn Reson Med* 55:700–705.
22. Chu B, Apfel RE (1982) Acoustic radiation pressure produced by a beam of sound. *The Journal of the Acoustical Society of America* 72:1673–1687.
23. Torr GR (1984) The acoustic radiation force. *American Journal of Physics* 52:402–408.
24. Nightingale K, McAleavey S, Trahey G (2003) Shear-wave generation using acoustic radiation force: in vivo and ex vivo results. *Ultrasound Med Biol* 29:1715–1723.
25. Larrat B, Pernot M, Aubry J-F, Sinkus R, Tanter M, Fink M (2008) Radiation force localization of HIFU therapeutic beams coupled with magnetic resonance-elastography treatment monitoring in vivo application to the rat brain. 2008 IEEE Ultrasonics Symposium. pp 451–454
26. McDannold N, Maier SE (2008) Magnetic resonance acoustic radiation force imaging. *Med Phys* 35:3748–3758.
27. Holbrook AB, Ghanouni P, Santos JM, Medan Y, Butts Pauly K (2011) In vivo MR acoustic radiation force imaging in the porcine liver. *Med Phys* 38:5081–5089.

28. Kaye EA, Chen J, Pauly KB (2011) Rapid MR-ARFI method for focal spot localization during focused ultrasound therapy. *Magn Reson Med* 65:738–743.
29. Larrat B, Pernot M, Aubry J-F, Dervishi E, Sinkus R, Seilhean D, Marie Y, Boch A-L, Fink M, Tanter M (2010) MR-guided transcranial brain HIFU in small animal models. *Phys Med Biol* 55:365–388.
30. Souchon R, Salomir R, Beuf O, Milot L, Grenier D, Lyonnet D, Chapelon J, Rouvière O (2008) Transient MR elastography (t-MRE) using ultrasound radiation force: Theory, safety, and initial experiments in vitro. *Magn Reson Med* 60:871–81.
31. Auboiroux V, Viallon M, Roland J, Hyacinthe J-N, Petrusca L, Morel DR, Goget T, Terraz S, Gross P, Becker CD, Salomir R (2012) ARFI-prepared MRgHIFU in liver: simultaneous mapping of ARFI-displacement and temperature elevation, using a fast GRE-EPI sequence. *Magn Reson Med* 68:932–946.
32. Bever JT de, Odéen H, Hofstetter LW, Parker DL (2018) Simultaneous MR thermometry and acoustic radiation force imaging using interleaved acquisition. *Magn Reson Med* 79:1515–1524.
33. Bitton RR, Kaye E, Dirbas FM, Daniel BL, Pauly KB (2012) Toward MR-guided high intensity focused ultrasound for presurgical localization: Focused ultrasound lesions in cadaveric breast tissue. *Journal of Magnetic Resonance Imaging* 35:1089–1097.
34. Bour P, Marquet F, Ozenne V, Toupin S, Dumont E, Aubry J-F, Lepetit-Coiffe M, Quesson B (2017) Real-time monitoring of tissue displacement and temperature changes during MR-guided high intensity focused ultrasound. *Magn Reson Med* 78:1911–1921.
35. Ilovitsh A, Fite BZ, Ilovitsh T, Ferrara KW (2019) Acoustic radiation force imaging using a single-shot spiral readout. *Phys Med Biol* 64:125004.
36. Qiao Y, Zou C, Chuanli C, Tie C, Wan Q, Peng H, Liang D, Liu X, Zheng H (2020) Simultaneous acoustic radiation force imaging and MR thermometry based on a coherent echo-shifted sequence. *Quantitative Imaging in Medicine and Surgery* 10:1823–1836.
37. Vappou J, Bour P, Marquet F, Ozenne V, Quesson B (2018) MR-ARFI-based method for the quantitative measurement of tissue elasticity: application for monitoring HIFU therapy. *Phys Med Biol* 63:095018.
38. Schmidt JL, Tweten DJ, Benegal AN, Walker CH, Portnoi TE, Okamoto RJ, Garbow JR, Bayly PV (2016) Magnetic resonance elastography of slow and fast shear waves illuminates differences in shear and tensile moduli in anisotropic tissue. *J Biomech* 49:1042–1049.
39. Kaye EA, Pauly KB (2013) Adapting MRI Acoustic Radiation Force Imaging For In Vivo Human Brain Focused Ultrasound Applications. *Magn Reson Med* 69:724–733.
40. Dadakova T, Krafft AJ, Özen AC, Bock M (2018) Optimization of acoustic radiation force imaging: Influence of timing parameters on sensitivity. *Magn Reson Med* 79:981–986.

41. D'Errico J (2012) Matlab functions: `fminsearchbnd`, `fminsearchcon` (<https://www.mathworks.com/matlabcentral/fileexchange/8277-fminsearchbnd-fminsearchcon>) MATLAB Central File Exchange.
42. Farrer AI, Odéen H, de Bever J, Coats B, Parker DL, Payne A, Christensen DA (2015) Characterization and evaluation of tissue-mimicking gelatin phantoms for use with MRgFUS. *J Ther Ultrasound* 3:9.
43. Cabras P, Auloge P, Bing F, Rao PP, Hoarau S, Dumont E, Durand A, Maurin B, Wach B, Cuvillon L, Breton E, Gangi A, Vappou J (2022) A new versatile MR-guided high-intensity focused ultrasound (HIFU) device for the treatment of musculoskeletal tumors. *Scientific Reports* 12:9095.
44. Lefebvre P, Tse Ve Koon K, Brusseau E, Nicolle S, Palierne J-F, Lambert S, Grenier D (2016) Comparison of Viscoelastic Property Characterization of Plastisol Phantoms with Magnetic Resonance Elastography and High-Frequency Rheometry. *Annu Int Conf IEEE Eng Med Biol Soc.* pp 1216–1219
45. Vappou J, Breton E, Choquet P, Goetz C, Willinger R, Constantinesco A (2007) Magnetic resonance elastography compared with rotational rheometry for in vitro brain tissue viscoelasticity measurement. *Magn Reson Mater Phy* 20:273.
46. Kruse SA, Smith JA, Lawrence AJ, Dresner MA, Manduca A, Greenleaf JF, Ehman RL, Kruse SA, Smith JA, Lawrence AJ, Dresner MA, Manduca A, Greenleaf JF (2000) Tissue characterization using magnetic resonance elastography: preliminary results. *Phys Med Biol* 45:1579–1590.
47. Sapin-de Brosses E, Gennisson J-L, Pernot M, Fink M, Tanter M (2010) Temperature dependence of the shear modulus of soft tissues assessed by ultrasound. *Phys Med Biol* 55:1701–1718.
48. Hofstetter LW, Odéen H, Bolster BD, Mueller A, Christensen D, Payne A, Parker DL (2019) Efficient shear wave elastography using transient acoustic radiation force excitations and MR displacement encoding. *Magn Reson Med* 81:3153–3167.
49. Hofstetter LW, Odéen H, Bolster BD, Christensen DA, Payne A, Parker DL (2021) Magnetic resonance shear wave elastography using transient acoustic radiation force excitations and sinusoidal displacement encoding. *Phys Med Biol* 66:055027.
50. Liu Y, Liu J, Fite BZ, Foiret J, Ilovitsh A, Leach JK, Dumont E, Caskey CF, Ferrara KW (2017) Supersonic transient magnetic resonance elastography for quantitative assessment of tissue elasticity. *Phys Med Biol* 62:4083–4106.
51. Chatelin S, Charpentier I, Corbin N, Meylheuc L, Vappou J (2016) An automatic differentiation-based gradient method for inversion of the shear wave equation in magnetic resonance elastography: specific application in fibrous soft tissues. *Phys Med Biol* 61:5000–5019.